Journal of Solid State Chemistry 186 (2012) 235–239

Contents lists available at SciVerse ScienceDirect

Journal of Solid State Chemistry

journal homepage: www.elsevier.com/locate/jssc

Controllable synthesis of a novel hedgehog-like core/shell structure

Shumin Wang [a], Hongwei Tian [a], Yanhui Pei [a], Qingnan Meng [a], Jianli Chen [a], Huan Wang [a], Yi Zeng [a], Weitao Zheng [a,*], Yichun Liu [b]

[a] Department of Materials Science, Key Laboratory of Mobile Materials, MOE, and State Key Laboratory of Superhard Materials, Jilin University, Changchun 130012, People's Republic of China

[b] Center for Advanced Optoelectronic Functional Materials Research and Key Laboratory for UV-Emitting Materials and Technology of Ministry of Education, Northeast Normal University, 5268 Renmin Street, Changchun 130024, People's Republic of China

ARTICLE INFO

Article history:
Received 22 October 2011
Received in revised form
12 December 2011
Accepted 14 December 2011
Available online 22 December 2011

Keywords:
Copper particles
Graphene encapsulated copper
RF-PECVD

ABSTRACT

A novel hedgehog-like core/shell structure, consisting of a high density of vertically aligned graphene sheets and a thin graphene shell/a copper core (VGs-GS/CC), has been synthesized via a simple one-step synthesis route using radio-frequency plasma-enhanced chemical vapor deposition (RF-PECVD). Scanning and transmission electron microscopy investigations show that the morphology of this core/shell material could be controlled by deposition time. For a short deposition time, only multilayer graphene shell tightly surrounds the copper particle, while as the deposition time is relative long, graphene sheets extend from the surface of GS/CC. The GS can protect CC particles from oxidation. The growth mechanism for the obtained GS/CC and VGs-GS/CC has been revealed. Compared to VGs, VGs-GS/CC material exhibits a better electron field emission property. This investigation opens a possibility for designing a core/shell structure of different carbon–metal hybrid materials for a wide variety of practical applications.

1. Introduction

Graphene is one of the most popular nanomaterials under intense investigation since it was obtained by Geim using a mechanical exfoliation method in 2004. Graphene is a two-dimensional honeycomb lattice material bonded with a single layer of sp^2-hybridized carbon atoms, exhibiting excellent physical properties, including quantum Hall effect, extremely high electronic mobility, thermodynamic stability, great elasticity, etc. [1–4]. Therefore, graphene offers great potential applications in field-effect transistors [5], vapor sensors [6], batteries [7–9], supercapacitors [10] and biosensors [11]. A hybrid of carbon shell and metallic core is a new material with the morphology different from nanotubes, fullerenes and graphene. The carbon shell could be either amorphous or graphitic [12–15]. Encapsulating a foreign material inside the carbon shell is of considerable significance. The carbon shell can protect the encapsulated metal from environmental degradation while retaining the intrinsic properties of the inside metal [15,16]. In addition, why the carbon shell–metallic core structure has been paid much attention is also due to their promising applications in the information technologies [17–19], biomedicines [20] and sensors [21]. Up till now, various techniques have been developed to synthesize the carbon encapsulated metal particles. Among them, standard and modified carbon arc discharge techniques are the most simple and popular methods [22]. Other methods include the pyrolysis of organometallic compounds, high-temperature annealing of mixtures of carbon-based materials and metal precursors, explosion and catalytic decomposition of methane, etc. [13,15–17,23–29]. The metal particles encapsulated with carbon, obtained by these methods, are all spheroidal on nanometer scales, in which the graphitic shells tightly surround the core metal nanoparticles. These encapsulated metal particles include magnetic or catalytic metals such as cobalt, nickel and iron [13,15,19], as well as the noble metals such as silver, platinum and gold [12]. It is worth noting that although Cu is a low-cost material but possesses good electric, optical and thermal properties, having a wide range of applications in the field of electronics, catalysis and optoelectronics [18,21], there are few reports about the preparation of the encapsulated copper metals, in particular, the carbon shell (such as GS)–copper core structure, which may be hard to be synthesized.

In this work, we try to obtain the hybrid of VGs and GS/CC using radio-frequency (RF) plasma enhanced chemical vapor deposition (PECVD) on Si(100) wafer, and the growth mechanism is revealed. This investigation may provide a possible way to synthesize a hybrid material of carbon shell and metal core, in which the metal can be either Cu or any other metal, in addition to Fe, Co, Ni, Pt, Ag and Au.

2. Experimental

2.1. Preparation of copper film

Cu film with a thickness of about 120 nm was deposited on Si(100) wafer by direct current magnetron sputtering. Prior to deposition, Si(100) substrate was cleaned in acetone, ethanol and

* Corresponding author. Fax: +86 431 85168246.
E-mail address: wtzheng@jlu.edu.cn (W. Zheng).

0022-4596/$ - see front matter © 2011 Elsevier Inc. All rights reserved.
doi:10.1016/j.jssc.2011.12.019

distilled water by ultrasonic for 15 min, respectively. The base pressure of the chamber was lower than 5×10^{-4} Pa. During deposition, the Ar gas pressure and the applied current on Cu target (99.95%) were 0.5 Pa and 0.1 A, respectively. The flow rate of Ar gas was kept at 60.0 sccm (sccm denotes standard cubic centimeters per minute at STP), accurately controlled by mass flow controller. The thickness for Cu film was determined by measuring the cross section of Cu thin film via scanning electron microscopy.

2.2. Synthesis of VGs-GS/CC hybrid material

After the Cu film was put into the reaction chamber of PECVD, the chamber was evacuated to a pressure of 10 Pa. Then a pressure of 220 Pa via introducing Ar (20 sccm) gas was maintained. As Cu film was heated to 800 °C and annealed for 10 min, Cu particles were formed. After that, the flow rate of Ar gas was changed to 50 sccm, and meanwhile, CH_4 with a flow rate of 20 sccm, acting as a carbon source, was introduced into the chamber. During deposition, the total pressure and discharge power were kept at 800 Pa and 200 W, respectively. After deposition, the obtained samples were cooled down to room temperature in Ar atmosphere.

2.3. Characterization

The crystal structure of copper was analyzed by X-ray diffraction (XRD) using a Bragg–Brentano diffractometer (D8_tools) in θ–2θ configuration with a Cu$K\alpha$ line at 0.15418 nm as a source, while the morphology and microstructure of the obtained materials were characterized by scanning electron microscopy (SEM) (JEOL JSM-6700 F), transmission electron microscopy (TEM), high resolution transmission electron microscopy (HRTEM) (JEOL JEM-2100F operated at 200 kV) and Raman spectra measurement (T64000 (Horiba), with a 514.5 nm Ar^+ laser excitation, a laser power of 7 mW, and an accumulation time of 30 s). Field-emission characteristics for the samples were carried out at a pressure of 2×10^{-4} Pa using a diode configuration at room temperature. An indium tin oxide (ITO) plate and sample with the size of 1 cm^2 mounted on Cu plate were used as the anode and cathode, respectively. The anode and cathode were separated by glass fibers with a diameter of 330 μm. Upon increasing the voltage between the two electrodes, a current flowing from samples to the ITO electrode was recorded.

3. Results and discussion

3.1. The microstructure and morphology of copper particles and VGs-GS/CC

Fig. 1 shows the XRD patterns for the Cu film (curve A), Cu particles (curve B) and VGs-GS/CC material grown for 6 min (curve C), 15 min (curve D) and 35 min (curve E), respectively, in which the broad peak from 41–45° in Fig. 1 (curve A) is from Cu(111), and the sharp peaks at 43.3° and 50.4° in curve B - E are assigned to Cu(111) and Cu(200), respectively, demonstrating that either Cu film or Cu particles has an fcc structure (JCPDS-ICDD Card No. 04-0836). In curves B–E, there are no reflections from either copper oxide or carbide, suggesting that the GS may protect the copper particles from oxidation in air, and the copper is chemically stable during graphene deposition. No graphite peak is observed because the diffraction signal from VGs-GS may be much lower than that of copper.

Figs. 2a and b exhibit the SEM images for Cu film before and after annealing. After heating to 800 °C, the Cu film with a thickness

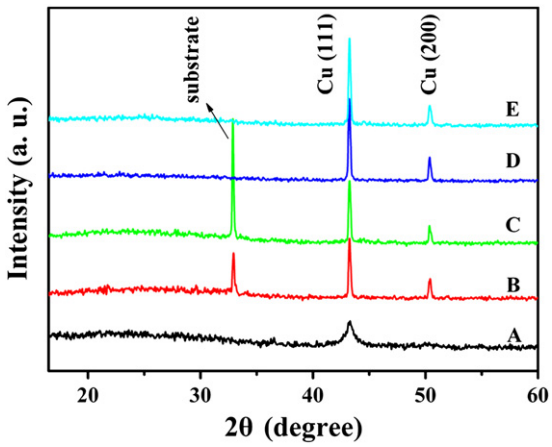

Fig. 1. XRD patterns for (A) Cu film, (B) Cu particles and VGs-GS/CC grown for (C) 6 min, (D) 15 min and (E) 35 min.

of about 120 nm became quasi-liquid and formed spherical islands caused by surface energy minimization through the liquid-like flow [30,31]. The Cu particles with a diameter of 100–700 nm are formed, randomly distribute on Si substrate and isolate from each other. Figs. 2c–e are the SEM images for the VGs-GS/CC deposited for 6, 15 and 35 min by using RF-PECVD, respectively. As the deposition time is 6 min, the surfaces of Cu particles are smooth with only a few small sizes of VGs (shown by the black arrow in Fig. 2c). However, as the deposition time is increased, more and more sharp VGs protrusions appear on the surfaces of copper particles, roughly vertically align on the surface of Cu particles, and become larger and larger. For a comparison, the graphene sheets roughly vertically grown on Si substrate (neither Cu film nor particles exists on Si(100) substrate) are exhibited in Fig. 2f. The graphene sheets grown on Cu particles are similar to those on Si substrate.

Fig. 3 displays the typical Raman spectra for the VGs-GS/CC materials and VGs prepared at different deposition times, in which there are two intense peaks between 1000 and 2000 cm^{-1}: D band (~1354 cm^{-1}) and G band (1586 cm^{-1}), which are the typical Raman peaks of graphene sheets (Gs). The D band originates from the corrugation of VGs, sp^3-hybridized carbon bonds in the VGs, and functional groups created by oxidation defects. The G band corresponds to the in-plane vibration of sp^2 carbon atoms (E_{2g}) [8]. Besides the G band, a distinct shoulder at 1620 cm^{-1} is attributed to D′ band, originating from finite-size graphite crystals, VGs edges and the presence of defects in the lattice, which is forbidden under defect-free conditions [32,33]. For a qualitative analysis of the VGs-GS/CC materials and VGs, the integrated intensity ratios of D over G band (I_D/I_G) are measured to define the degree of crystallinity of the carbonaceous materials. The smaller the I_D/I_G is, the higher the degree of graphitization is. From Fig. 3, I_D/I_G values for VGs-GS/CC grown for 6 (curve A), 15 (curve B) and 35 (curve C) min are calculated to be 2.13, 1.84 and 1.56, respectively, which are bigger than that of the VGs (1.48) grown on Si substrate (curve D). As the deposition time increases, the degree of graphitization increases and the crystal defects decrease in VGs-GS/CC. The strong G and D bands indicate that the obtained VGs-GS/CC and VGs have a graphitic structure with some crystal defects, ascribing to etching and destroying VGs from ion bombardment during PECVD.

Figs. 4a–c show the TEM images of VGs-GS/CC grown for 6, 15 and 35 min, respectively, from which the size as well as vertical length of each VGs is enlarged with increasing deposition time. The vertical length of these VGs grown on Cu surface for 35 min is 100–150 nm. The inset in Fig. 4c is a high-resolution TEM (HRTEM) image

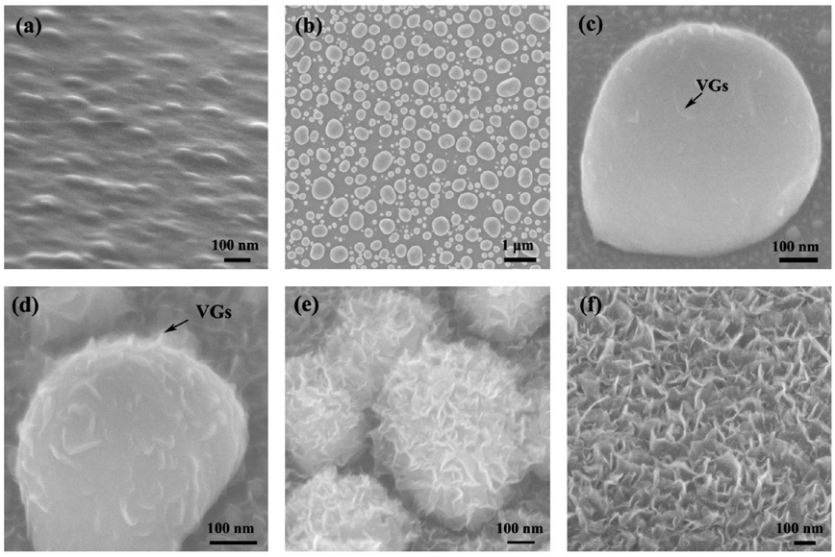

Fig. 2. SEM images for Cu films (a) before and (b) after annealing, SEM images for VGs-GS/CC grown for (c) 6 min, (d) 15 min, and (e) 35 min, respectively, and (f) SEM image for VGs grown on Si substrate without Cu.

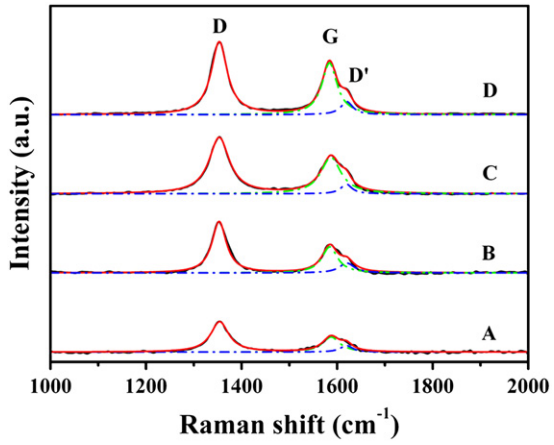

Fig. 3. Raman spectra of VGs-GS/CC grown for (A) 6, (B) 15, (C) 35 min, and (D) VGs grown on Si substrate without Cu for 35 min. Curve fitting of the spectra around the second peak is also shown.

at the edge of VGs, which exhibits that the obtained VGs on Cu particles have a thickness of less than 10 nm. The spacing between neighboring graphene layers is about 0.34 nm, in a good agreement with the interplanar distance of (002) graphite [8]. Figs. 4d–e, f–h and i are the HRTEM images of VGs-GS/CC grown for 6, 15 and 35 min, respectively, in which the interplanar spacing for Cu particles is 0.175 and 0.206 nm, agreeing well with that of (200) and (111) plane, respectively, for Cu with fcc structure [14]. Figs. 4f–h show that graphene shells with the interlayer spacing of about 0.34–0.38 nm tightly surround the Cu core without any obvious voids between the core and shell. A small protrusion of multi-layer graphene appears on GS, indicated by a white arrow in Fig. 4d, which has not been observed in the HRTEM images of VGs-GS/CC grown for 2 min. Fig. 4g exhibits that a graphene nanosheet with a small size extends from the surface of GS/CC with a compatible contact with GS for VGs-GS/CC grown for 15 min. Moreover, no oxides can be observed in Figs. 4e, f and i, indicating that GS has protected these Cu cores from oxidation.

From SEM, TEM and HRTEM images, it can be confirmed that a novel hedgehog-like material with a VGs-GS/CC structure is obtained. The carbon shells are formed by two parts: the first part just near the "core" consists of a few layer of graphene, which can be proved by the HRTEM images in Fig. 4, and the second part outside consists of highly dense graphene sheets vertically grown on a hybrid of GS/CC. These two parts are compatible with each other so well, proved by Figs. 4g and h. This can be ascribed to that these two parts are all bonded with sp^2-hybridized carbon atoms. A hybrid particle in VGs-GS/CC sample damaged by the knifepoint during the preparation of the SEM sample is shown in Fig. 5a, and an enlarged image (Fig. 5b) is marked with a box, in which we can clearly observe a smooth surface for the Cu particle. In Figs. 5a and b, the inner surface of the VGs-GS is smooth, and the graphene sheets are indeed roughly vertically grown on the Cu particle. This provides another proof that the two parts of the shell are compatible with each other tightly.

However, the mechanism for the formation of these two parts is different. As is schematically illustrated in Fig. 6, the growth of VGs-GS/CC consists of three stages: (1) after heating to 800 °C and annealing for 10 min, Cu film changes into well-dispersed and spheroidal particles; (2) a plasma power (200 W) is applied to decompose methane into carbon radicals (CH_x^+, species impinging from gas phase in plasma, $x=0$, 1, 2, 3,) and hydrogen. The extremely high concentration of carbon radicals causes a solution of C in Cu. If the deposition time is short, only GS tightly surrounds the Cu core particles after cooling, while as the deposition time is relatively long, the carbon dissolved in the Cu particles becomes supersaturated. Meanwhile, VGs begin to nucleate and grow up. At an initial state, nucleation sites are enlarged to form planar graphene sheets on Cu surface. When two growing graphene sheets meet each other, graphene sheets are forced to rise upwards, causing the formation of VGs [32,34]. The active H radicals tend to spread on the surface of Cu, protecting the Cu particles from oxidation, and can rapidly remove away the amorphous carbon defects in VGs, remaining a high degree of graphitization structure. The atomic hydrogen also etches the edge of VGs to keep them thin; (3) afterwards, in the process of cooling, carbon atoms segregate from the interior of Cu particles to form graphene layers at the interlayer between Cu and VGs. Consequently, VGs-GS/CC material is obtained.

As mentioned above, we can obtain either Cu particles encapsulated with multilayer graphene or VGs-GS/CC structure via choosing a proper deposition time. Our findings provide an important guidance

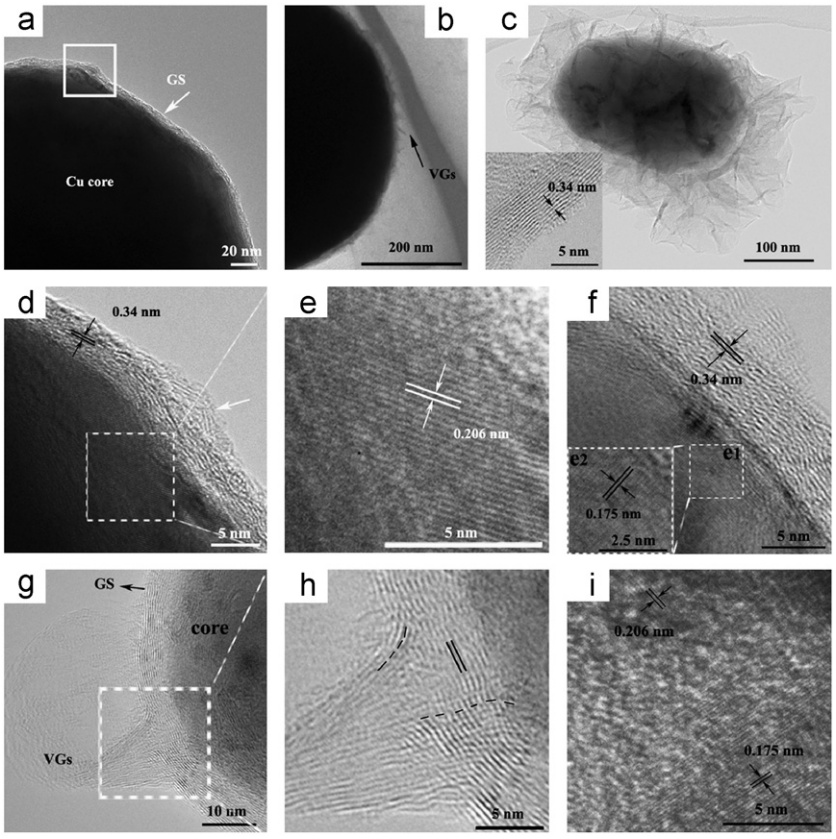

Fig. 4. TEM images of VGs-GS/CC grown for (a) 6 min, (b) 15 min and (c) 35 min. The inset HRTEM image in (c) shows the edge of VGs, where the adjacent lattice spacing is 0.34 nm. Corresponding to the area indicated with a box in (a), the HRTEM images are shown in (d) and (e); to that in (b), the HRTEM images are exhibited in (f), (g), and (h); to that in (c), the HRTEM image is displayed in (i).

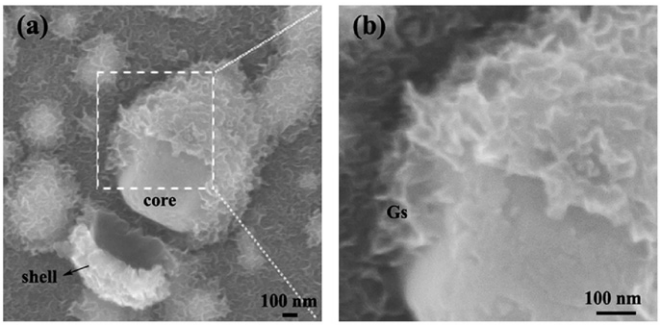

Fig. 5. (a) SEM image for a damaged hybrid particle of VGs-GS/CC grown for 35 min, and (b) an enlarged region indicated by a box in (a).

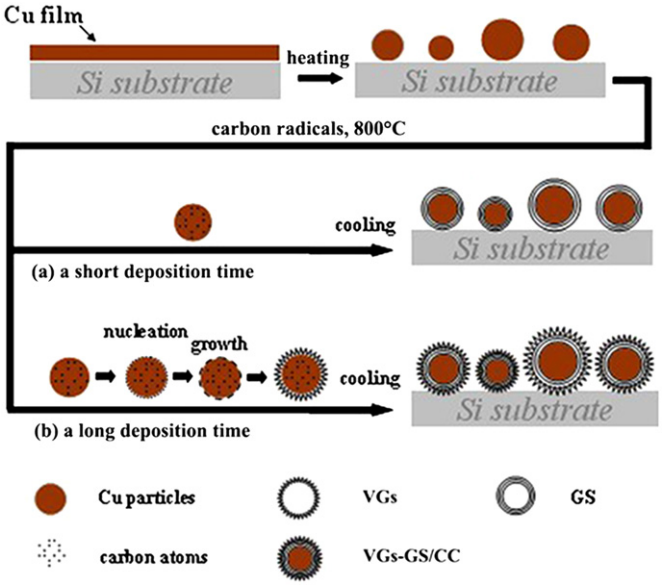

Fig. 6. Schematic illustrations for the formation mechanism of GS/CC and VGs-GS/CC.

toward encapsulating a foreign metal without catalytic property inside the graphitic material shells.

3.2. The field electron emission properties of VGs-GS/CC

Fig. 7 displays the current density (J) as a function of applied electric field (E) for VGs directly grown on Si substrate (curve A) and VGs-GS/CC (curve B) material. The turn-on electric fields at 1 $\mu A/cm^2$ are estimated approximately to be 3.8 and 4.5 V/μm, respectively, and under the same applied electric field, the emission current density of VGs-GS/CC is larger, compared to that of VGs, which indicates that the obtained VGs-GS/CC exhibits a better field emission property than VGs. The Fowler–Nordheim (FN) plots of the field electron emissions for VGs (curve A) and VGs-GS/CC (curve B) shown in the inset of Fig. 7 can well describe the field emission behaviors of the samples. FN plots roughly fit to the linear relationship given by $\ln(J/E^2)=\ln(A\beta^2/\Phi)-B\Phi^{3/2}/\beta E$, where A and B are constants ($A=1.54\times10^{-6}$ A eV V^{-2}, $B=6.83\times10^3$ $eV^{-3/2}$ $V\mu m^{-1}$), $\beta$the dimensionless field enhancement factor and Φ the work function of emitters [35–37]. Here, the Cu particles on Si substrate produced by annealing do not display a

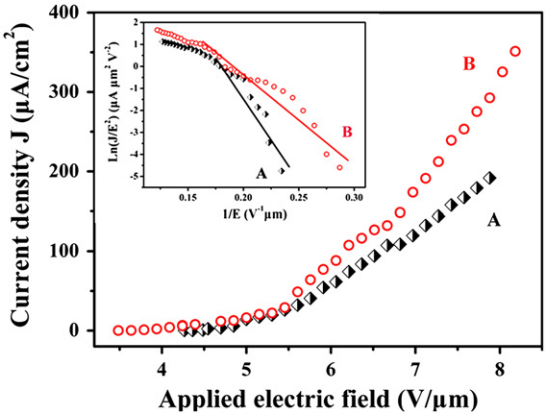

Fig. 7. FE current density vs applied electric field for (A) VGs directly grown on Si(100) for 35 min and (B) VGs-GS/CC grown for 35 min, in which the inset exhibits the F–N plots corresponding to (A) and (B), respectively.

field electron emission. Therefore, the field electron emissions of samples are attributed primarily to the VGs (Φ for VGs is ~5.0 eV) [35]. From the slope of the FN plots, the field enhancement factor β for VGs and VGs-GS/CC grown on Si substrate can be estimated to be about 1020 and 1850, respectively, on average. The bigger the enhancement factor β, the better the field emission property. According to the Raman spectra in Fig. 3, there is no apparent difference in the bonding structure of carbon atoms between VGs and VGs-GS/CC. Hence we believe that the field emission enhancement of VGs-GS/CC, compared to VGs grown on Si substrate, can be attributed to the geometrical factors such as a high density of emitters (more sharp edges) on Cu particles that randomly distribute on Si substrate. As for VGs-GS/CC, the VGs on Cu particles are closer to the anode and the 'field shielding' effect among VGs is weak due to a large separation between VGs on different Cu particles.

4. Conclusions

Vertically aligned graphene sheets-graphene shell/copper core (VGs-GS/CC) material has been successfully prepared by using RF-PECVD technique. The Cu cores are formed by thermally annealing the Cu thin film grown by direct current magnetron sputtering. We find that the morphology of VGs-GS/CC material could be controlled by choosing proper deposition time, and VGs-GS/CC material exhibits an improved FE property, compared to VGs grown on Si substrate. Therefore, it is reasonable to expect that this novel material has a potential application in field emission devices.

Acknowledgments

The support from National Natural Science Foundation of China (Grant nos. 50525204, 50832001 and 51002061), the special Ph.D. program (Grant no. 200801830025) from MOE, program for Changjiang Scholars and Innovative Research Team in University, and the "211" and "985" project of Jilin University, China, is highly appreciated.

References

[1] K.S. Novoselov, A.K. Geim, S.V. Morozov, D. Jiang, Y. Zhang, S.V. Dubonos, G. IV, A.A. Firsov, Science 306 (2004) 666–669.
[2] A.K. Geim, K.S. Novoselov, Nat. Mater. 6 (2007) 183–191.
[3] Y.B. Zhang, Y.W. Tan, H.L. Stormer, P. Kim, Nature 438 (2005) 201–204.
[4] A.K. Geim, Science 324 (2009) 1530–1534.
[5] V. Ryzhii, M. Ryzhii, Phys. Rev. B 79 (2009) 245311.
[6] A.T.C. Johnson, Y.P. Dan, Y. Lu, N.J. Kybert, Z.T. Luo, Nano Lett. 9 (2009) 1472–1475.
[7] Y.G. Guo, B. Wang, X.L. Wu, C.Y. Shu, C.R. Wang, J. Mater. Chem. 20 (2010) 10661–10664.
[8] S.M. Wang, Y.H. Pei, X. Wang, H. Wang, Q.N. Meng, H.W. Tian, X.L. Zheng, W.T. Zheng, Y.C. Liu, J. Phys. D: Appl. Phys. 43 (2010) 455402.
[9] L.J. Zhi, X. Wang, K. Mullen, Nano Lett. 8 (2008) 323–327.
[10] R.S. Ruoff, M.D. Stoller, S.J. Park, Y.W. Zhu, J.H. An, Nano Lett. 8 (2008) 3498–3502.
[11] J.H. Li, Y. Wang, Y.Y. Shao, D.W. Matson, Y.H. Lin, ACS Nano 4 (2010) 1790–1798.
[12] C.S. Yoon, J.H. Kim, C.K. Kim, Y.H. Kim, Colloids Surf. A 321 (2008) 297–300.
[13] S.H. Jeong, J.B. Park, M.S. Jeong, J.Y. Kim, B.K. Cho, Carbon 46 (2008) 1369–1377.
[14] A. Gedanken, D.S. Jacob, I. Genish, L. Klein, J. Phys. Chem. B 110 (2006) 17711–17714.
[15] Y. Lu, Z.P. Zhu, Z.Y. Liu, Carbon 43 (2005) 369–374.
[16] X.L. Dong, Z.D. Zhang, S.R. Jin, B.K. Kim, J. Appl. Phys. 86 (1999) 6701–6706.
[17] X.G. Liu, Z.Q. Ou, D.Y. Geng, Z. Han, J.J. Jiang, W. Liu, Z.D. Zhang, Carbon 48 (2010) 891–897.
[18] X.L. Dong, X.F. Zhang, H. Huang, D.K. Wang, J.P. Lei, Nanotechnology 18 (2007) 275701.
[19] J.A. Blanco, M.P. Fernandez-Garcia, P. Gorria, M. Sevilla, M.P. Proenca, R. Boada, J. Chaboy, A.B. Fuertes, J. Phys. Chem. C 115 (2011) 5294–5300.
[20] Y.H. Lin, D. Du, Z.X. Zou, Y.S. Shin, J. Wang, H. Wu, M.H. Engelhard, J. Liu, I.A. Aksay, Anal. Chem. 82 (2010) 2989–2995.
[21] E.K. Athanassiou, R.N. Grass, W.J. Stark, Nanotechnology 17 (2006) 1668–1673.
[22] J.M. Bonard, S. Seraphin, J.E. Wegrowe, J. Jiao, A. Chatelain, Chem. Phys. Lett. 43 (2001) 251–257.
[23] N. Nishi, J. Nishijo, C. Okabe, O. Oishi, Carbon 44 (2006) 2943–2949.
[24] H.P. Wang, C.H. Huang, J.E. Chang, E.M. Eyring, Chem. Commun. (2009) 4663–4665.
[25] U. Narkiewicz, M. Podsiadly, Appl. Surf. Sci. 256 (2010) 5249–5253.
[26] N.W. Jian, Z. Li, Y. Fan, M.S. Zhao, J. Phys. Chem. B 111 (2007) 2119–2124.
[27] A. Ermoline, M. Schoenitz, E. Dreizin, N. Yao, Nanotechnology 13 (2002) 638–643.
[28] M. Nagatsu, Q. Ou, T. Tanaka, A. Mesko, A. Ogino, Diam. Relat. Mater. 17 (2008) 664–668.
[29] S.H. Tsai, C.L. Lee, C.W. Chao, H.C. Shih, Carbon 38 (2000) 781–785.
[30] T. Ichinokawa, H. Itoh, Y. Sakai, J. Anal. At. Spectrom. 14 (1999) 405–408.
[31] N. Eustathopoulos, P. Protsenko, J.P. Garandet, R. Voytovych, Acta Mater. 58 (2010) 6565–6574.
[32] W.H. Liu, T. Dang, Z.H. Xiao, X. Li, C.C. Zhu, X.L. Wang, Carbon 49 (2011) 884–889.
[33] J.L. Gong, Q.T. Li, Z.C. Ni, D.H. Zhu, Z.Y. Zhu, Carbon 46 (2008) 434–439.
[34] M.Y. Zhu, J.J. Wang, B.C. Holloway, R.A. Outlaw, X. Zhao, K. Hou, V. Shutthanandan, D.M. Manos, Carbon 45 (2007) 2229–2234.
[35] J. Hwang, M.Y. Chen, C.M. Yeh, J.S. Syu, C.S. Kou, Nanotechnology 18 (2007) 185706.
[36] Y.M. Ho, G.M. Ynag, W.T. Zheng, X. Wang, H.W. Tian, Q. Xu, H.B. Li, J.W. Liu, J.L. Qi, Q. Jiang, Nanotechnology 19 (2008) 065710.
[37] W.T. Zheng, G.M. Yang, X. Wang, Q. Xu, S.M. Wang, H.W. Tian, J. Solid State Chem. 182 (2009) 966–972.